Effects of Precipitation on the Upper-Ocean Response to a Hurricane

S. DANIEL JACOB

Goddard Earth Science and Technology Center, University of Maryland, Baltimore County, Baltimore, and NASA Goddard Space Flight Center, Greenbelt, Maryland

CHESTER J. KOBLINSKY

NOAA Climate Office, Silver Spring, Maryland

(Manuscript received 22 March 2006, in final form 22 June 2006)

ABSTRACT

The effect of precipitation on the upper-ocean response during a tropical cyclone passage is investigated using a numerical model in this paper. For realistic wind forcing and empirical rain rates based on satellite climatology, numerical simulations are performed with and without precipitation forcing to delineate the effects of freshwater forcing on the upper-ocean heat and salt budgets. Additionally, the performance of five mixing parameterizations is also examined for the two forcing conditions to understand the sensitivity of simulated ocean response. Overall, results from 15 numerical experiments are analyzed to quantify the precipitation effects on the oceanic mixed layer and the upper ocean. Simulated fields for the same mixing scheme with and without precipitation indicate a decrease in the upper-ocean cooling of about 0.2°–0.5°C. This is mainly due to reduced mixing of colder water from below induced by the increased stability of the added freshwater. The cooler rainwater contributes a maximum of approximately 10% to the total surface heat loss from the ocean. The rate of freshening due to precipitation exceeds the rate of mixing of the more saline water from below, leading to a change in sign of the mixed layer salinity response. As seen in earlier studies, large uncertainty exists in the simulated upper-ocean response due to the choice of mixing parameterization. Although the nature of simulated response remains similar for all the mixing schemes, the magnitude of freshening and cooling varies by as much as 0.5 psu and 1°C between the schemes to the right of the storm track. While changes in the mixed layer and in the top 100 m of heat and salt budgets are strongly influenced by the choice of mixing scheme, integrated budgets in the top 200 m are seen to be affected more by advection and surface fluxes. However, since the estimated surface fluxes depend upon the simulated sea surface temperature, the choice of mixing scheme is crucial for realistic coupled predictive models.

1. Introduction

Tropical cyclones represent one of the most destructive natural disasters known to mankind. The primary energy source driving these storms is the latent heat release due to the condensation of water vapor, which ultimately comes from the ocean. As a storm intensifies, increasing wind speed may increase evaporation and supply the storm with the necessary source of heat for further intensification. However, with increasing wind speed, oceanic vertical mixing reduces sea surface temperature (SST) causing a reduction of sea surface fluxes. Past studies have focused on this negative feedback as part of the spreading three-dimensional wake (Chang and Anthes 1978). Estimates of cooling induced by vertical mixing in the oceanic mixed layer (ML) heat budget have ranged from about 70% from observations (Jacob et al. 2000, hereafter JSMB) to as high as 99% in a coupled ocean–atmosphere model simulations (Bender et al. 1993). Additionally, prestorm ocean features such as warm core eddies and ocean currents also affect the upper-ocean cooling (Jacob and Shay 2003).

Understanding the impact of these factors in the mutual interaction of the tropical cyclone–ocean is central to more accurately forecasting intensity change in landfalling tropical cyclones (Marks et al. 1998). However,

Corresponding author address: S. Daniel Jacob, Goddard Earth Science and Technology Center, University of Maryland, Baltimore County, 5523 Research Park Dr., Suite 320, Baltimore, MD 21228.
E-mail: jacob@umbc.edu

DOI: 10.1175/MWR3366.1

© 2007 American Meteorological Society

effects of precipitation on the upper-ocean heat and salt budgets during hurricane passage have not been investigated in detail in the past due to obvious measurement difficulties of rain rates in the inner core of tropical cyclones. Based on climatological rainfall estimates of Miller (1958) and average precipitation temperatures consistent with those found by Gosnell et al. (1995) in the western Pacific, JSMB estimated a 10% contribution to the heat flux by rain-induced cooling. However, the addition of fresh rainwater at a rate exceeding 15 mm h^{-1} into the ocean mixed layer will also significantly affect static stability and therefore modulate ocean mixing. Hence, in this paper, the effect of rainfall on upper-ocean heat and salt budgets is investigated using a high-resolution numerical model for forcing associated with hurricane Gilbert (1988) in the Gulf of Mexico for quiescent initial conditions. For five commonly used oceanic mixing schemes, the spatial evolution of mixed layer tracers is also examined to quantify the magnitude of variability. The paper is organized as follows: in section 2, details of the numerical model, initial conditions, forcing, and numerical experiments are presented, followed by the effects of precipitation on the upper-ocean heat and salt budgets in section 3 for different mixing parameterizations. Results are summarized in section 4. As the focus of this paper is on the precipitation effects, detailed evaluation of the mixing schemes and comparisons with data will be presented in a forthcoming paper.

2. Numerical model

The Hybrid Coordinate Ocean Model (HYCOM) is used in this study. This is a primitive equation, ocean general circulation model that was developed from the Miami Isopycnic Coordinate Ocean Model (MICOM) to provide higher vertical resolution in regions with weak stratification, including the surface mixed layer and in relatively shallow water regions with varying topography, especially when tidal and wind forcing mixes the water column from the surface to the bottom (Bleck 2002). The open-ocean vertical grid in HYCOM consists of fixed-level coordinates confined close to the ocean surface that transition smoothly to isopycnic coordinates in the ocean interior preserving the advantages of isopycnic coordinates throughout as much of the water column while resolving the surface boundary layer with fixed-level depth coordinates. The interior isopycnic coordinates are allowed to collapse to zero thickness at the bottom. The HYCOM vertical grid is also designed to horizontally transition from depth and isopycnic coordinates in the ocean interior to terrain-following σ coordinates in shallow-water regions. This enables vertically continuous higher-order mixing parameterizations to be implemented in the model (Halliwell 2004).

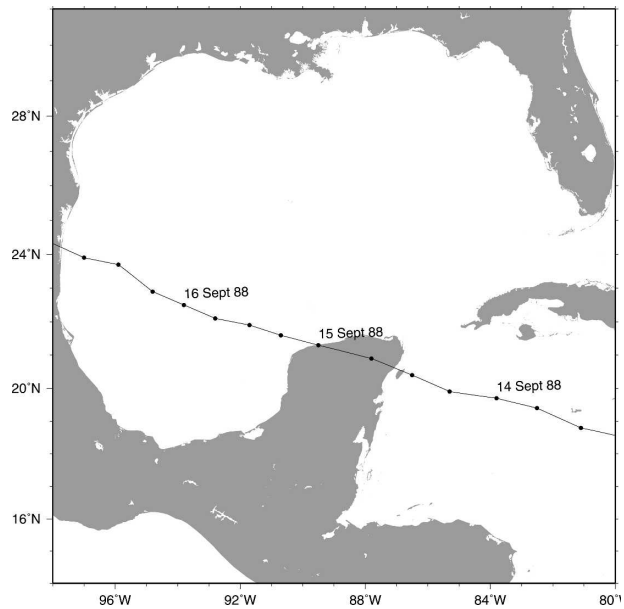

FIG. 1. Geographic area covered by the model domain. The solid line represents the track of the hurricane. Storm center locations every 6 h are denoted by the dots, and the dates for 0000 UTC positions are labeled.

a. Configuration

The model domain used in this study extends from 14°–31°N to 80°–98°W (Fig. 1) similar to our earlier MICOM study in the Gulf of Mexico (Jacob and Shay 2003). With a horizontal grid resolution of 0.07°, the model has 250 × 242 horizontal grid points and 50 coordinate levels in the vertical. In the present version, layer densities are chosen to represent the Gulf of Mexico during September (midhurricane season) with z levels in the upper ocean held at a minimum distance of 3 m. The bathymetry used in the model is derived from the 5-Minute Gridded Earth Topography Data (ETOPO5) topography and the boundaries along the Florida Straits and the Caribbean Sea are closed by vertical sidewalls as we focus on the upper-ocean response in the Western Gulf of Mexico.

b. Initial conditions

In the Gulf of Mexico model domain used in this study, major features of oceanic circulation include the Loop Current and the warm mesoscale eddies that separate from it. The water mass associated with these features has a distinct temperature–salinity (T–S) relationship in contrast to the Gulf Common Water

(GCW). Earlier studies have documented the importance of realistic initialization of the ocean model for more accurate ocean response simulation due to hurricane passage (JSMB; Jacob and Shay 2003). However, as the main focus of the present study is to understand the role of precipitation on the upper-ocean response and its effect on the choice of vertical mixing parameterizations, it was decided to initialize the model with quiescent conditions. Following Jacob and Shay (2003), vertical temperature structure from a prestorm airborne expendable bathythermograph (AXBT) during Hurricane Gilbert (1988) provided the oceanic condition in the upper 1000 m and the corresponding salinities are estimated from the historical *T–S* relationship of GCW. The *T–S* relationship of the model vertical profile is shown in Fig. 2. While the salinity is constant in the upper 100 m, the maximum salinity is approximately at a depth of 220 m.

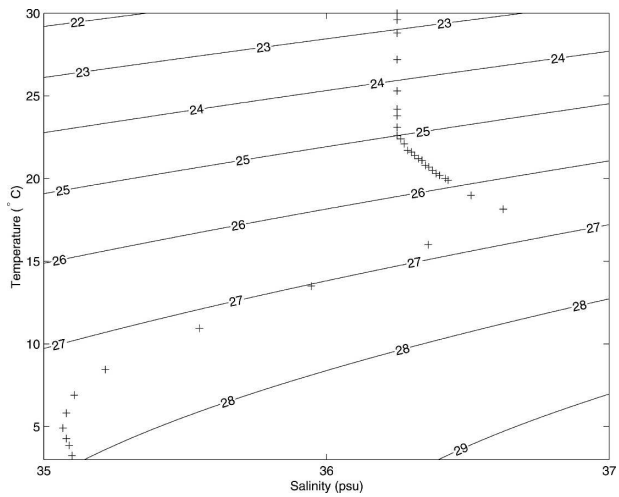

FIG. 2. The *T–S* relationships in the Gulf of Mexico corresponding to the GCW in the model.

c. Surface forcing

Air–sea exchanges of momentum and heat are estimated using the bulk aerodynamic formulas to provide mechanical and thermal forcing in the model:

$$\boldsymbol{\tau} = C_D U_{10} \mathbf{U}_{10} \rho_a, \tag{1}$$

$$Q_S = C_H U_{10} (T_{\mathrm{ss}} - T_{10}) \rho_a C_{\mathrm{pa}}, \tag{2}$$

$$Q_L = C_E U_{10} (q_{\mathrm{ss}} - q_{10}) \rho_a L_{\mathrm{va}}, \tag{3}$$

where $\boldsymbol{\tau} = \tau_x \mathbf{i} + \tau_y \mathbf{j}$ is the wind stress vector, assumed to be aligned along the surface wind vector at 10 m ($U_{10} = |\mathbf{U}_{10}|$), Q_S is the sensible heat flux, T_{10} is the air temperature at 10 m, T_{ss} is the air temperature at the sea surface assumed to be the SST, Q_L is the latent heat flux, q_{10} is the specific humidity of air at 10-m height, and q_{ss} is the specific humidity at the sea surface assuming saturation at a given SST.

The surface drag coefficient (C_D) was computed using a wind speed–dependent formulation of Large and Pond (1981): $C_D = 1.14 \times 10^{-3}$ for $U_{10} \leq 10$ m s^{-1} or $(0.49 + 0.065U_{10}) \times 10^{-3}$ for $U_{10} > 10$ m s^{-1}. While recent studies show that the drag coefficient levels off at high wind speeds (Powell et al. 2003; Shay and Jacob 2006), for the wind speeds associated with hurricane Gilbert in the Gulf of Mexico, use of this linearly increasing relationship does not significantly affect the ocean response (Shay and Jacob 2006). Constant values of 1×10^{-3} for the sensible heat flux coefficient (C_H) and 1.2×10^{-3} for the latent heat flux coefficient (C_E) are used because of the near neutrality of the atmospheric boundary layer in hurricanes. Parameters ρ_a, C_{pa}, and L_{va} represent density of air, heat capacity of air, and latent heat of vaporization, respectively.

Surface winds needed to estimate fluxes are derived using observations in the domain. During Gilbert's passage in the Gulf of Mexico, two National Oceanic and Atmospheric Administration (NOAA) WP-3D aircraft acquired wind and thermodynamic measurements at a flight level of 850 hPa at least twice a day in the inner-core area of the storm. These data indicated flight-level, 10-min sustained winds of about 52–58 m s^{-1} in the Gulf of Mexico. A National Data Buoy Center (NDBC) 10-m discus buoy (42002) at 25.89°N, 93.57°W, which was approximately 300 km to the right of Gilbert's track, acquired surface wind speed, wind direction, pressure, air temperature, and SST at hourly intervals during Gilbert. These data provide information in and near the core of the storm. However, to obtain boundary layer winds over the entire Gulf of Mexico, information about the environmental flow is also needed. The European Centre for Medium-Range Weather Forecasts (ECMWF) model surface dataset is used in this study to provide the background wind field. This model-generated surface field has a spatial resolution of 1.125° × 1.125° and radiosonde-acquired atmospheric observations are assimilated into the model on a regular basis. The model surface wind field is then blended with the aircraft and buoy observations to generate boundary layer winds every 3 h (JSMB; Powell and Houston 1996) to provide the surface forcing for ocean model simulations (Fig. 3). A constant air temperature of 26°C and relative humidity of 85% at 10 m are assumed to estimate latent and sensible heat fluxes (Black 1983).

Precipitation rates used in this study are estimated using climatological information and individual storm

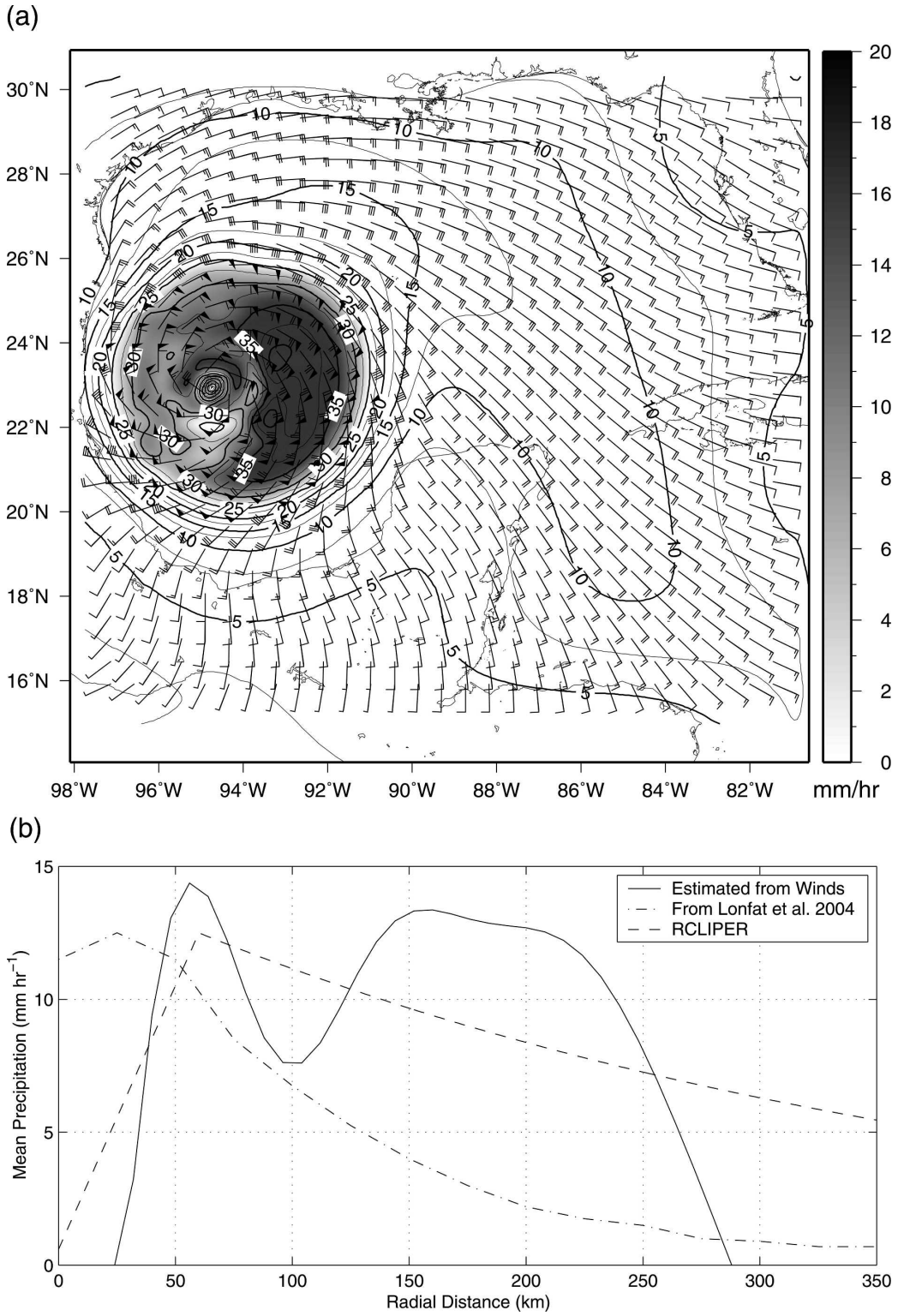

FIG. 3. (a) Surface winds derived from flight level–reduced, ECMWF surface, and buoy winds for 0600 UTC 16 Sep 1988. Every eighth data point from the analyzed field is plotted as a barb (kt) with contours representing the wind magnitudes in m s^{-1}. Gray shades represent derived rain rates in mm h^{-1}. (b) Comparison of the axisymmetric mean rain rates used in this study with the TMI rainfall climatology and the RCLIPER model. While the maximum rain rate is not collocated with R_{max} in the climatology, this radius is chosen to be R_{max} for RCLIPER.

observations. Lonfat et al. (2004) based on the Tropical Rainfall Measuring Mission (TRMM) Microwave Imager (TMI) data derived the radial distribution of mean rain rates as a function of storm intensity. In this mean climatology, the maximum axisymmetric mean rainfall of 12.5 mm h^{-1} was at a distance of 25 km from the storm center for category-3–5 storms. However, this mean climatology cannot be used directly in this study because a rain maximum at 25 km will not be collocated with the primary eyewall. In addition, Gilbert was intensifying to a category-4 storm and undergoing an eyewall replacement cycle with stronger winds in the secondary eyewall, therefore the Rainfall Climatology and Persistence (RCLIPER) model (Marks et al. 2002) may not be representative of the precipitation structure with its single rain maximum at the radius of maximum winds. TMI observations of Hurricane Floyd (1999) at category 4 undergoing eyewall replacement cycle show intense rain in excess of 25 mm h^{-1} in the primary eyewall and a rain rate of 15 mm h^{-1} in the secondary eyewall with a relative minima in between (see Fig. 2 of Lonfat et al. 2004). A similar structure was also seen in hurricane Dennis (1999) by Lonfat et al. (2004). Based on this information, the prescribed rain rates are scaled by the analyzed wind field in this study. A maximum rain rate of 16 mm h^{-1} is assigned for wind speeds greater than 35 m s^{-1} that is linearly reduced to 0 mm h^{-1} at 25 m s^{-1}. The distribution of winds and the rain rates are shown in Fig. 3a for the surface forcing corresponding to 0600 UTC 16 September 1988. The axisymmetric mean rain rates estimated using this procedure are compared with the mean values of Lonfat et al. (2004) and the RCLIPER model–predicted rain rates with R_{max} as the maximum rainfall radius in Fig. 3b. While the peak values estimated are higher by about 2 mm h^{-1} than the TMI-observed mean, they are comparable to values in the primary eyewall of Hurricane Dennis (1999) and less than those in Hurricane Floyd (1999; see Figs. 2 and 5 of Lonfat et al. 2004). It is likely the procedure used in this study will overestimate rain rates between the inner and outer eyewalls; however, the first-order precipitation effects will be better reproduced, as the derived rain rates are more representative of the storm structure.

In the model results examined in detail in this study, the temperature of rainwater is assumed to be the sea surface temperature for simplicity. However, the colder rainwater contributes to sensible heat loss in the upper ocean. For a rain temperature of T_{rain}, this sensible heat loss can be expressed as

$$Q_R = C_{pw} R (T_{ss} - T_{rain}), \tag{4}$$

where R is the rain rate, C_{pw} is the heat capacity of water, and T_{rain} is the rain temperature. The rain temperature can be assumed to be the wet-bulb temperature (assumption found to be good to 0.1 K in the tropical Pacific by Gosnell et al. 1995) and for the air temperature and humidity values used in this study, T_{rain} = 24.04°C. Therefore the maximum sensible heat loss for a rain rate of 16 mm h^{-1} ($R = 4.4 \times 10^{-3}$ K gm^{-2} s^{-1}) is Q_R = 110 W m^{-2}, approximately 10% of the maximum surface heat loss of 1200 W m^{-2}. Since this additional heat loss also affects the stability of the water column, a set of numerical simulations is performed to quantify this sensitivity.

d. Vertical mixing parameterizations

Presently there is a choice of five mixing schemes in HYCOM. These can be broadly classified into two categories: higher-order schemes that provide mixing from the surface to the bottom and slab models where the predicted mixing is generally confined to the near-surface mixing zone. Details of the implementation of these schemes in HYCOM are explained in Halliwell (2004) and are only briefly reviewed here. The K-profile parameterization (KPP; Large et al. 1994), one of the primary schemes used in HYCOM is a higher-order scheme in which many physical processes are parameterized to provide mixing. This scheme also parameterizes the influence of nonlocal convective mixing of temperature and salinity that can lead to countergradient fluxes. Two other higher-order schemes implemented in HYCOM and investigated here are the National Aeronautics and Space Administration (NASA) Goddard Institute of Space Studies (GISS) level-2 turbulence closure scheme (Canuto et al. 2001; 2002) and the Mellor–Yamada (MY) level-2.5 scheme (Mellor and Yamada 1982). In the GISS scheme, viscosity and diffusivity coefficients are obtained by solving the second-order moments and parameterizing the turbulent kinetic energy (TKE) dissipation rates for different dynamic stability regimes while in the MY scheme TKE (q^2) and TKE times the turbulence length scale ($q^2 l$, instead of dissipation ϵ) are used to estimate viscosity and diffusivity profiles. The MY is the only scheme in HYCOM that accounts for the horizontal advection and diffusion of turbulence (Halliwell 2004).

The two slab mixing schemes in HYCOM are the Price–Weller–Pinkel (PWP; Price et al. 1986) and the Kraus–Turner (KT; Kraus and Turner 1967; Gaspar 1988) parameterizations. In the PWP scheme, vertical mixing is performed for three unstable conditions: static instability, dynamic instability due to the bulk Richardson number falling below 0.65, and dynamic in-

stability due to the gradient Richardson number values of 0.25 and below. In the KT scheme, TKE generated by stress and buoyancy at the surface is balanced by the mixing of denser water into the mixed layer. Numerical simulations are performed for these schemes to understand the sensitivity of simulated oceanic heat and salt budgets to precipitation forcing.

e. Numerical experiments

As described in the previous sections, the numerical model is initialized with the quiescent condition and the ocean response due to the mechanical and thermal forcing is investigated. Numerical experiments are conducted with and without the precipitation forcing for the five mixing schemes to quantify the variability due to precipitation and examine the performance of the different mixing schemes. The set of numerical experiments performed is listed in Table 1. The model is integrated for forcing corresponding to 6 days from 0000 UTC 14 September to 0000 UTC 20 September 1988 and simulated temperature, salinity, and currents are compared between individual cases.

TABLE 1. Details of numerical experiments.

Case	Precipitation forcing	Mixing scheme
KPN	No	KPP
KTN	No	KT
PWN	No	PWP
MYN	No	MY
GIN	No	GISS
KPP	Yes	KPP
KTP	Yes	KT
PWP	Yes	PWP
MYP	Yes	MY
GIP	Yes	GISS
KPT	Yes with rain temperature	KPP
KTT	Yes with rain temperature	KT
PWT	Yes with rain temperature	PWP
MYT	Yes with rain temperature	MY
GIT	Yes with rain temperature	GISS

3. Results

a. Precipitation effects

Evolution of mixed layer temperature and salinity are first investigated with and without freshwater forcing for one mixing scheme to quantify the range of simulated variability. As the KPP scheme is commonly used in HYCOM, simulated fields from cases KPN (without precipitation) and KPP are discussed in the following section with respect to the initial conditions. The effect of cooler precipitation temperatures on the upper ocean is simulated in case KPT and discussed relative to case KPP. Spatial variability induced by the freshwater forcing is quantified by examining the upper-ocean temperature and salinity response from the two snapshots in the directly forced and relaxation stages of the ocean response, respectively.

1) SEA SURFACE TEMPERATURE RESPONSE

Due to the quiescent initialization of the ocean model, mixed layer temperatures (MLTs; sea surface temperature and mixed layer temperature are used interchangeably in this paper as the difference between the two is negligible here) remained a constant 30°C in the domain prior to the arrival of forcing associated with storm. With the arrival of winds in the western Gulf of Mexico one day into the model integration, MLTs start to reduce ahead of the storm due to mixing of cooler water from below. There is a significant rightward bias in the MLT response as seen in past observational and modeling studies (Shay et al. 1992; Black 1983; Price 1981). The magnitude of cooling between 2 and 3 R_{max} (i.e., the radius of maximum winds, 60 km in this case) is a maximum of 4.5°C in the right-rear quadrant of the storm. It is clearly seen from the snapshots in the directly forced region that the MLT evolution remains similar between cases KPN and KPP (Figs. 4a,c). In the central Gulf of Mexico, away from topographic influences, the MLT difference due to precipitation remained at approximately 0.2°C with the higher MLT values in case KPN. This reduction in MLT cooling with the added freshwater forcing is only due to the reduction in the mixing of cooler water from below the mixed layer base as the precipitation temperature is taken to be the same as that of MLT in this case. Observations in the tropical western Pacific indicate this temperature may be up to 4°C cooler than the MLT (Gosnell et al. 1995; Anderson et al. 1998). While such data are not available for hurricane rainfall, as mentioned earlier, the wet-bulb temperature is a good approximation for this temperature. This effect is included in case KPT and the results show a maximum difference of ~0.03°C (not shown). Although this additional cooling reduces static stability, the overall effect on the MLT is small because the maximum contribution of this heat loss to the total surface heat flux is only on the order of 10%. The simulated difference of 0.2°C in MLT between KPP and KPN contributes to a small difference in the heat fluxes to the atmosphere as estimated by the bulk formulas. Upper-ocean thermal response remains similar with comparable differences two days after the storm's passage.

2) SEA SURFACE SALINITY RESPONSE

The prestorm sea surface/mixed layer salinity (SSS/MLS) is a constant 36.25 psu in the domain estimated

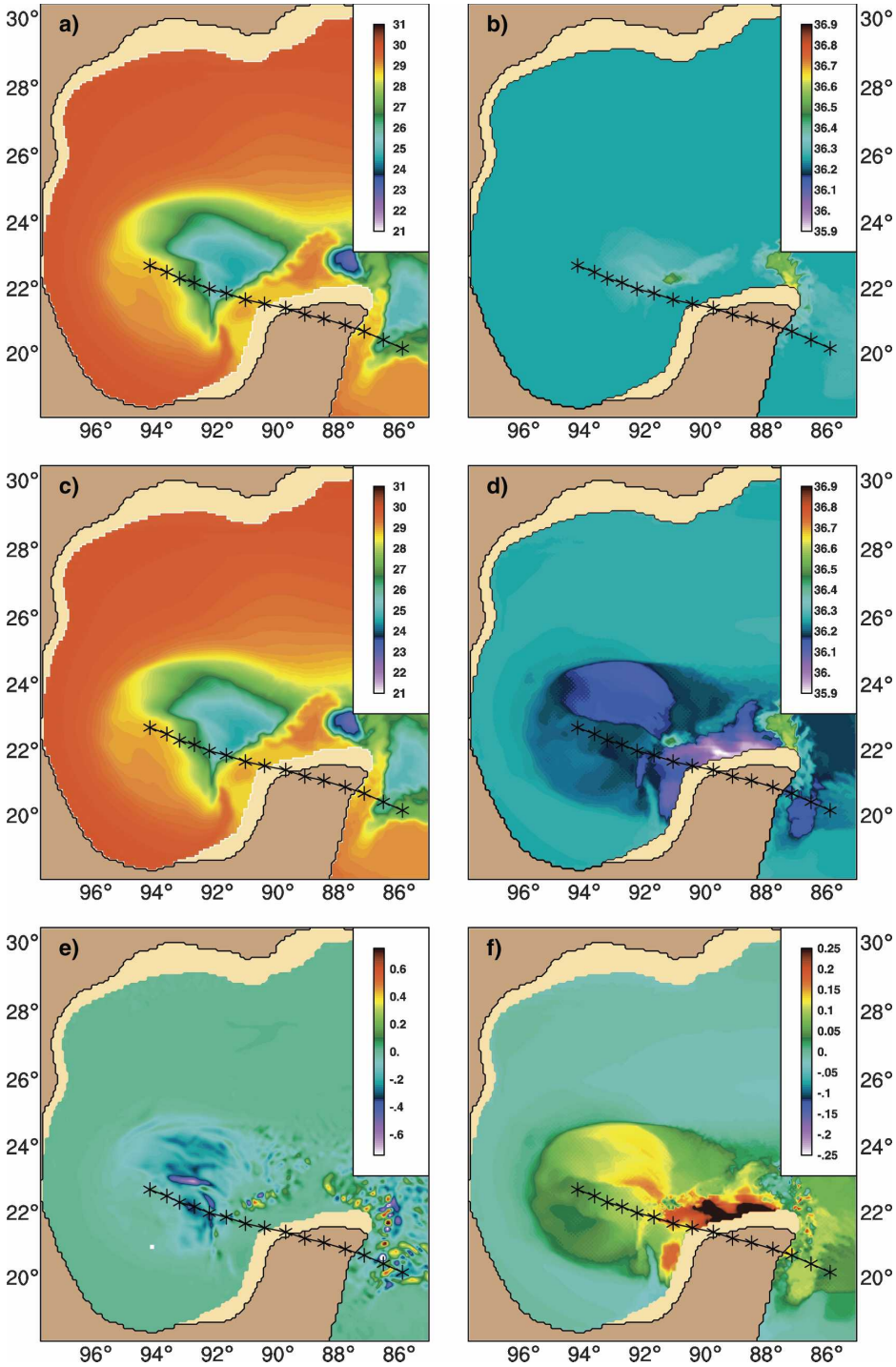

FIG. 4. Simulated MLTs and MLSs in cases KPN and KPP in the directly forced region: (a) KPN MLT, (b) KPN MLS, (c) KPP MLT, (d) KPP MLS, (e) ΔMLT (KPN − KPP), and (f) ΔMLS (KPN − KPP). Note the differences in the simulated MLS between the two cases.

from the climatological *T*–*S* relationship for the GCW in the Gulf of Mexico (Fig. 2). In contrast to the MLT response, the MLS response is very different when precipitation is included in the forcing. Without precipitation, relatively more saline water from below is entrained into the mixed layer leading to MLS increases in the directly forced region. When precipitation is added to forcing, the freshwater input reduces the ef-

fective salinity that results in increased stability of the water column. This requires a larger TKE to simulate comparable mixing rates seen in the no precipitation case. While the salinity increases in the case of no freshwater forcing are confined very close to the storm track, lower salinity values are found as far away as $4R_{max}$ to the right of the storm center in the directly forced region when precipitation forcing is considered (Figs. 4c,d). Quantitatively, a maximum difference of about 0.3 psu in the MLS is estimated from these results consistent with observations from the Tropical Cyclone Motion Experiment (TCM90) by Pudov and Ginis (2000). The simulated MLS virtually remains the same in case KPT where the precipitation temperature effects are included as in case KPP. With the Aquarius SSS mission to be launched in 2009, lower salinity signatures due to these extreme freshwater forcing will be observed from space and can be used as a supplemental information to validate rain rates estimated through other microwave and radar observations. Similar to the cooler MLTs, freshwater signature persists at the surface two days after the storm's passage advected away from the track by the storm-induced currents (not shown). Additionally, simulated currents and mixed layer depths are not significantly affected by freshwater forcing. However, the choice of vertical mixing scheme in the ocean model has been shown to be a source of large simulated upper-ocean variability and therefore this issue is investigated in detail in the following section.

b. Sensitivity to vertical mixing schemes

As discussed in the previous section, simulated upper-ocean response in cases KPN and KPP indicated the importance of freshwater forcing. While the oceanic mixed layer (OML) is expected to be fresher when rain forcing is added, the important result from these simulations is that the rate of freshening is higher than the rate of mixing from below resulting in a fresher mixed layer compared to the initial state. In this section, the simulated ocean response for all five mixing schemes with and without precipitation forcing is examined first in the directly forced region. Temporal evolution of mixed layer quantities and upper-ocean heat and salt content is investigated at a location $2R_{max}$ to the right of the storm track because of the strong ocean response in this region. Additionally, evolution of average quantities within a $5R_{max}$ radius with respect to the storm center on 0600 UTC 16 September 1988 is also examined to quantify the variability within the storm footprint as this is important in coupled predictive models of hurricane intensity.

1) DIRECTLY FORCED REGIME

The spatial structure of simulated MLT and MLS in the directly forced region for the four remaining mixing schemes with and without precipitation forcing is shown in Figs. 5 and 6, respectively. While the asymmetry of the ocean response is similar for all the schemes, MLTs simulated for the three higher-order schemes remain remarkably similar with and without precipitation forcing. As seen between cases KPN and KPP, use of freshwater forcing reduces the MLT cooling by 0.2°C between cases GIN and GIP and MYN and MYP. While the magnitude of simulated cooling in cases KTN and KTP remains the smallest (Fig. 5a), cooling is much larger in cases PWN and PWP than in the other simulations. This is due to stronger simulated mixing by the PWP scheme used in these two cases. This result is further confirmed by the spatial structure of simulated MLS in case PWN, where more saline water from below is entrained into the mixed layer over a larger area (Fig. 6b). In case PWP, however, due to the increased static stability of the water column, temperature and salinity converge toward values from other simulations. In contrast, due to less intense mixing, the mixed layers remain less saline in the other three cases (KTN, MYN, and GIN) without precipitation forcing (Figs. 6a,c,d). While the freshwater forcing–induced MLS freshening has a maximum magnitude of 0.25 psu in comparison to the no precipitation cases, the lesser the predicted mixing, the fresher the OML remains. By examining the temporal evolution of OML quantities, differences due to the five mixing schemes are further quantified.

2) TIME EVOLUTION

(i) Sea surface temperature response

Evolution of mixed layer quantities to the right of the storm where ocean response is the strongest, highlights the variability introduced due to precipitation and mixing schemes. Without taking into account the precipitation forcing, the lowest and highest values of MLTs are simulated in cases KTN and PWN, respectively (Fig. 7a). Simulated MLTs in the five cases start to diverge in the directly forced region beyond -0.5 t/IP (time defined with respect to 0600 UTC 16 September 1988 normalized by the inertial period of 30 h) ahead of the point of closest approach of the storm center. A maximum difference in MLT of up to 2.5°C is seen between cases PWN and KTN at 0.5 t/IP that corresponds to the right-rear quadrant. This tendency is maintained farther along the wake during the relax-

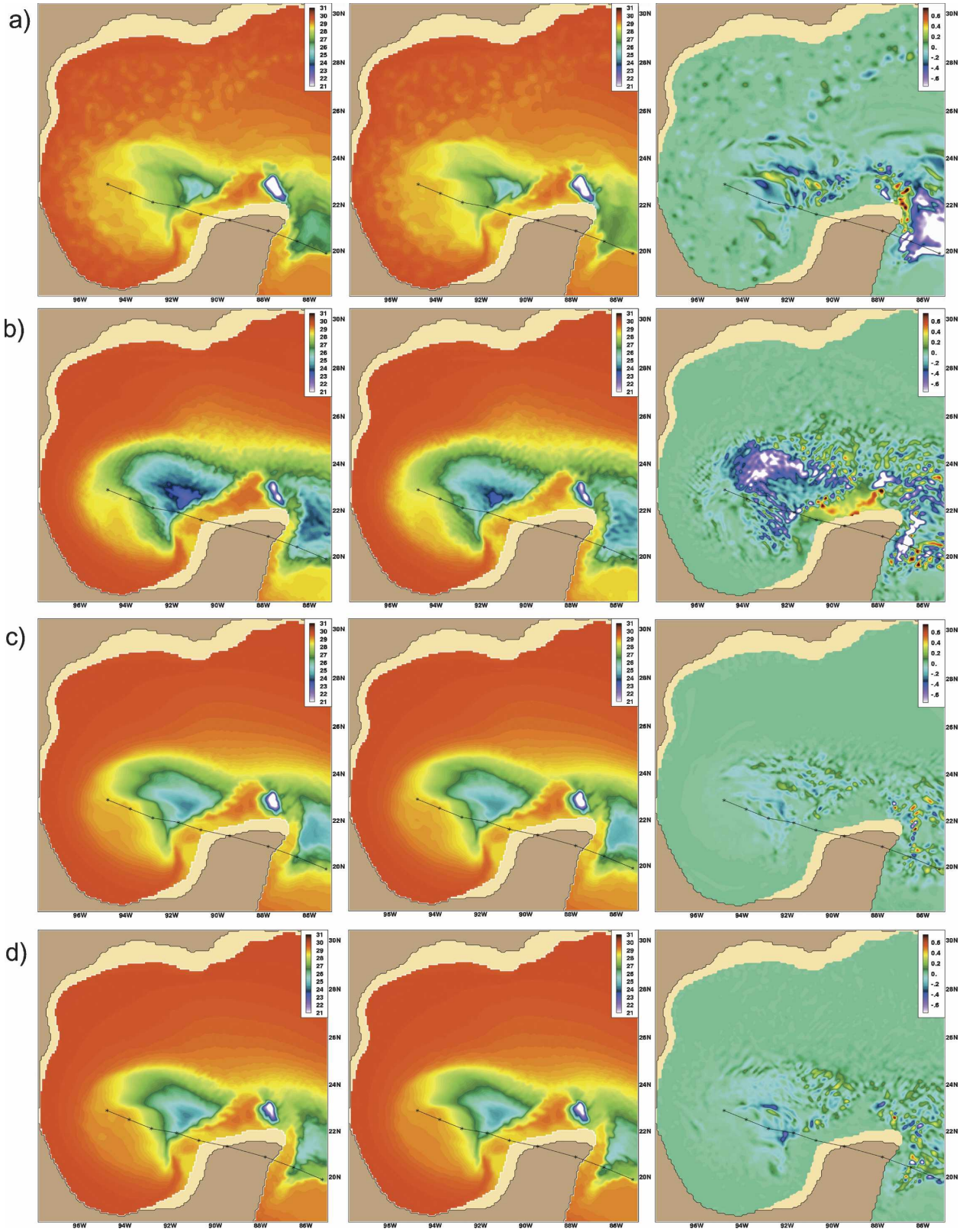

FIG. 5. Snapshots of simulated MLT for the additional four mixing schemes. (left) No precipitation forcing, (middle) with precipitation forcing, and (right) the difference (left − center) between the two. Results in each row are for (a) Gaspar (KTN and KTP), (b) PRT (PWN and PWP), (c) MY (MYN and MYP), and (d) GISS (GIN and GIP) schemes. Differences of more than 0.50°C are found for the PRT scheme in the region of interest. The black line represents the storm track with the 6-hourly storm center marked by asterisks.

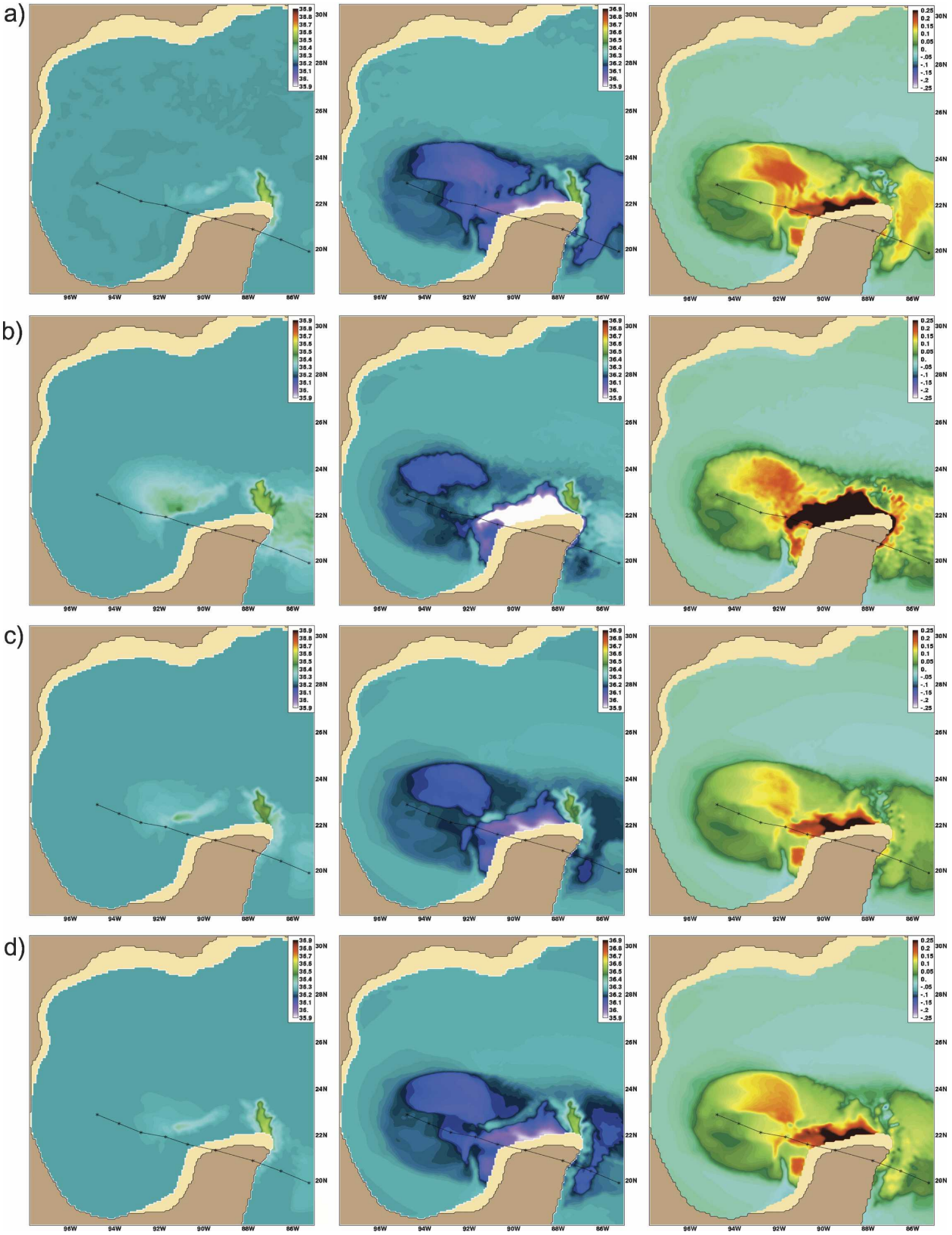

FIG. 6. Same as in Fig. 5, but for snapshots of simulated MLS for the four different mixing schemes. The higher-order mixing schemes have a similar behavior compared to the other two schemes. The black line represents the storm track.

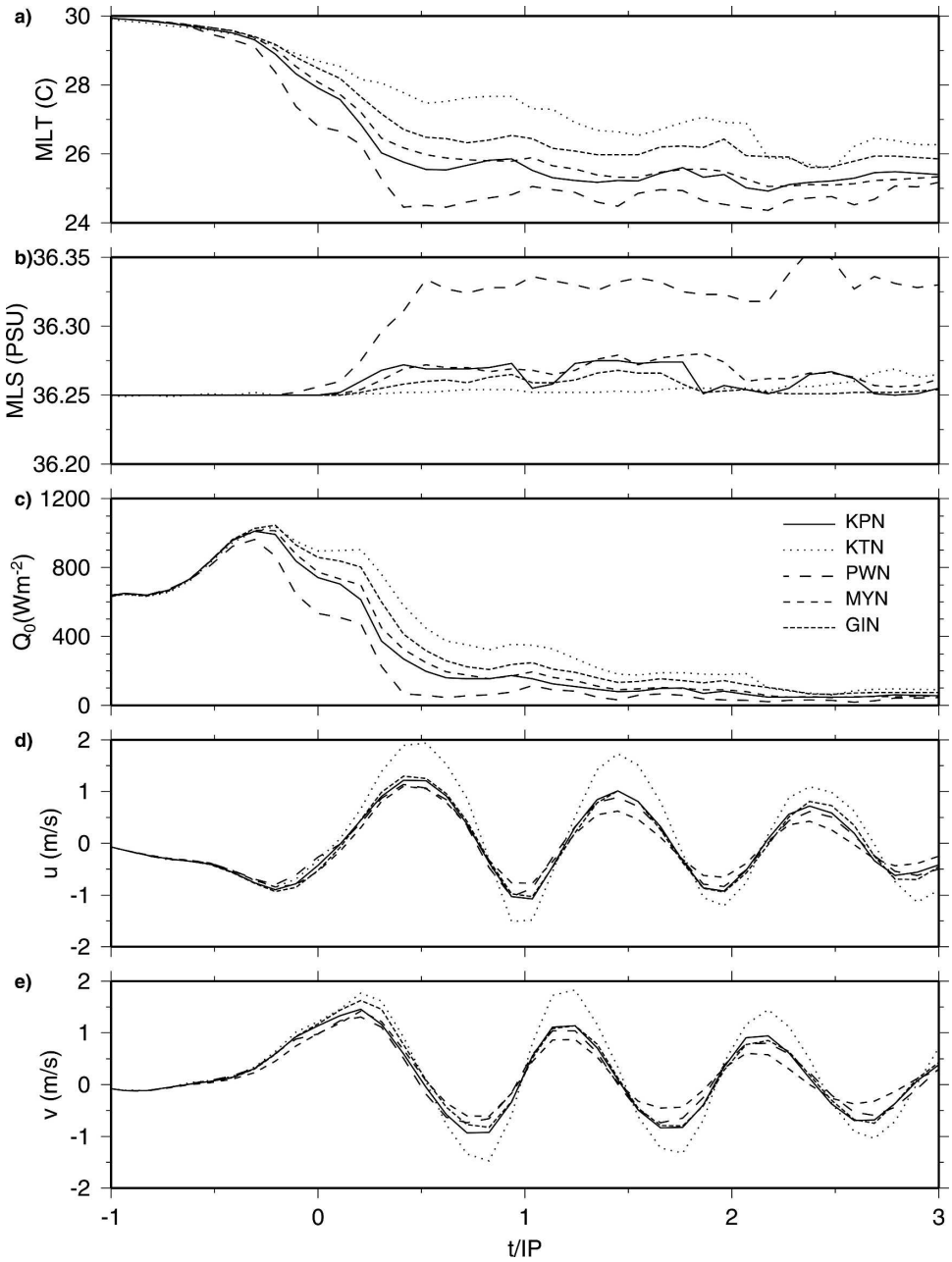

FIG. 7. Evolution of the mixed layer response at a location $2R_{max}$ to the right of the storm track in the Gulf of Mexico without precipitation forcing. The time axis is normalized by the inertial period at that latitude (30 h): (a) MLT, (b) MLS, (c) surface heat flux, (d) u, and (e) v.

ation stage (beyond 0.5 t/IP) though the differences become smaller. In the other three cases where higher-order schemes are used, simulated MLTs are in the range between those in PWN and KTN with much lower differences among the three. While the MLTs are clearly advected by the horizontal currents associated with a near-inertial oscillation, significant differences induced by the strong forcing appear beyond a wind speed of 20 m s^{-1} at -0.5 t/IP ahead of the storm center. When precipitation is added to the forcing, a similar trend remains in the simulated MLTs with about 0.5°C reduction in the spread between cases PWP and KTP (Fig. 8a). Additionally, the effect of precipitation temperature–induced sensible heat loss is negligible in the directly forced region although minor differences are apparent beyond 0.5 t/IP (Fig. 10a).

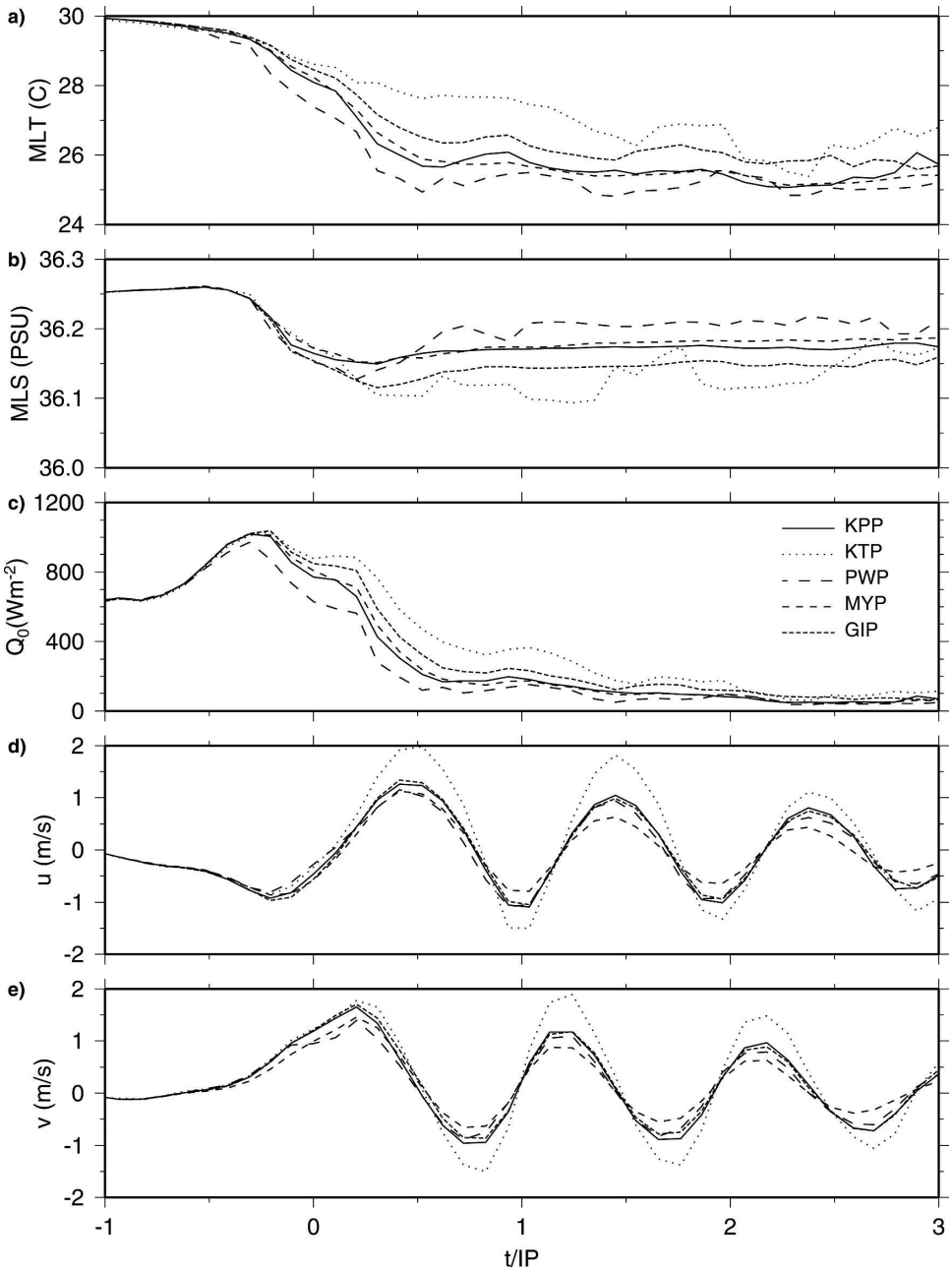

FIG. 8. Same as in Fig. 7 but with precipitation forcing: (a) MLT, (b) MLS, (c) surface heat flux, (d) *u*, and (e) *v*.

(ii) Sea surface salinity response

The MLS evolution for the two forcing conditions at this location highlights the effect of precipitation on the upper-ocean salt budget. In the no-precipitation condition, MLS simulated by all mixing schemes remain similar ahead of the storm center. Beyond 0 *t*/IP however, MLS in the PWN case increases significantly in the right-rear quadrant (0–0.5 *t*/IP) due to enhanced mixing (Fig. 7b). While in the other cases the simulated MLS evolution is clustered together, MLS changes are minimal in case KTN due to less intense mixing. When precipitation forcing is used, MLS starts to decrease at −0.5 *t*/IP ahead of the storm with a maximum freshening seen in the KTP case relative to other cases (Fig. 8b). As mentioned earlier, freshening of the mixed layer due to precipitation increases static stability, which leads to a simulated MLS in the PWP case that is

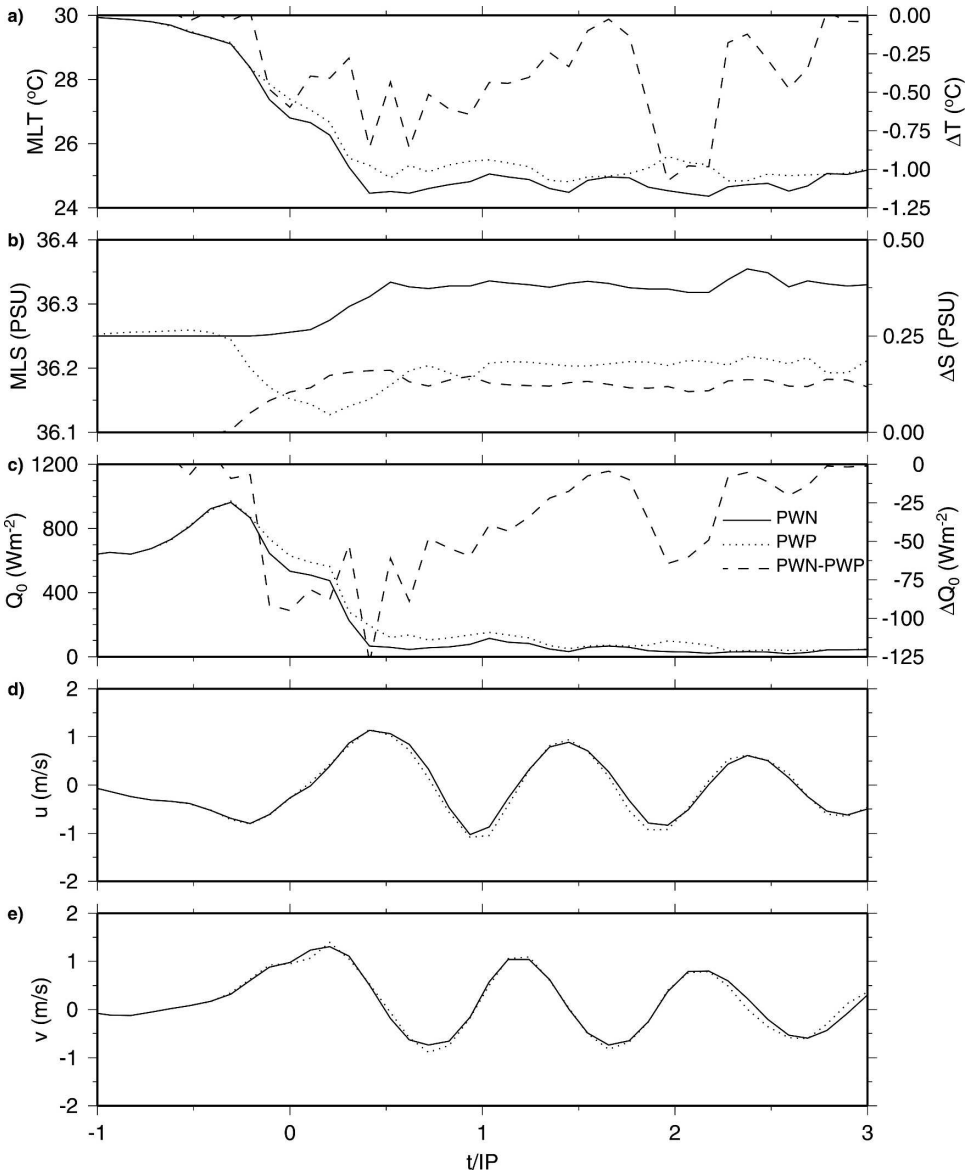

FIG. 9. Evolution of the mixed layer response at a location $2R_{max}$ to the right of the storm track in the Gulf of Mexico in cases PWN and PWP: (a) MLT and ΔMLT, (b) MLS and ΔMLS, (c) surface heat flux (Q_0) and ΔQ_0, (d) u, and (e) v.

more consistent with the other schemes (Fig. 8b). The MLT and MLS evolution in cases PWN and PWP are compared quantitatively in Fig. 9, which clearly shows a mean temperature and salinity differences of 0.5°C and 0.2 psu in the mixed layer. Additionally, an average freshening of 0.2 psu is seen in the wake of the storm in all the five cases when precipitation forcing was used (Fig. 8b). Similar to the MLT variability, the precipitation temperatures have a minimal effect on the MLS evolution (Fig. 10b). As indicated by the MLT and MLS evolution, results from the three higher-order schemes do not differ significantly from each other.

(iii) Surface fluxes

One of the important factors in coupled hurricane track and intensity prediction models is the surface flux from the ocean to the atmosphere. Simulated values of this heat flux vary significantly between the five schemes with a maximum difference of 400 W m^{-2} in the directly forced region (Fig. 7c). Since the heat fluxes here are estimated using bulk formulas assuming constant air temperature and humidity values at 10 m, estimated fluxes are only dependent on simulated MLTs and wind speeds. With the wind speed being the same

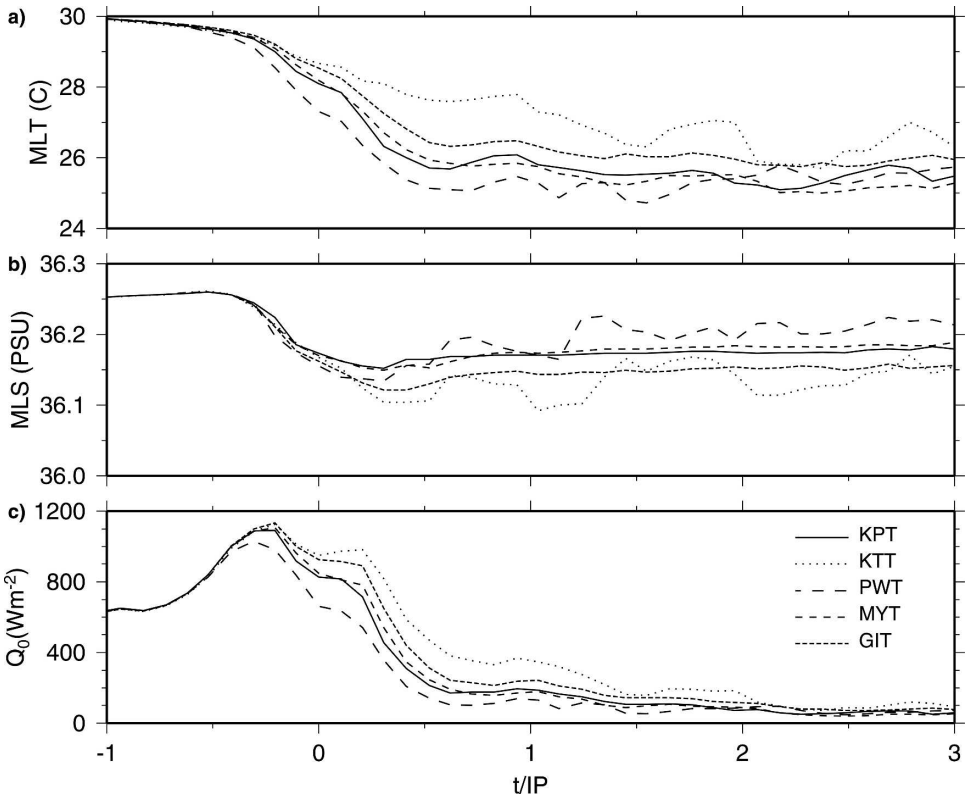

FIG. 10. Evolution of mixed layer response at a location $2R_{max}$ to the right of the storm track in the Gulf of Mexico with precipitation forcing including the effect of sensible heat loss due to lower precipitation temperatures. (a) MLT; (b) MLS; and (c) surface heat flux.

in all cases, fluxes in case PWN are the smallest. In contrast, fluxes are largest in the KTN case directly reflecting the MLT changes. Similar tendencies persist in the OML up to the end of the integration with minor differences between the five schemes. With added precipitation there is a slight increase in fluxes with a marginal reduction in the spread between the five cases (Fig. 8c). When the precipitation temperature effects are included, the maximum total heat loss increases by about 100 W m^{-2} and there is a marginal increase in the spread between the cases as seen in Fig. 10c.

Averaged currents in the mixed layer are in quadrature and ranged from 1 to 2 m s^{-1} between the five mixing schemes where the effect of precipitation is minimal (Figs. 7d,e, and 8d,e). With lower MLDs in the KTN and KTP cases, simulated currents are much higher than other schemes. A similar behavior of the KT scheme was also seen in a previous study (Jacob and Shay 2003). For a fast moving storm as the one considered here, fluxes needed to intensify and maintain generally come from within the directly forced region. The magnitude and variability of MLT and MLS within the storm footprint is quantified to estimate the range of variability due to the choice of these mixing schemes. The results are shown in Table 2. In general, the MLT change in this region is assumed to be 1°C and for all the mixing schemes indeed the average remains close to this value. Precipitation effects on this average are also minimal. However, a difference of 0.4°C seen

TABLE 2. Changes in the average MLT and MLS within the storm footprint covered by a circle of radius $5R_{max}$ with respect to the storm center at 0600 UTC 16 Sep 1988. A difference of 0.4°C is seen between PWN and GIN. The coolest and most saline mixed layer is simulated in case PWN. While the more saline mixed layers are seen in cases PWN and PWP at $2R_{max}$, the mixed layer in case KPP is saltier than others in the directly forced region with added precipitation.

Case	ΔT (°C)	ΔS (PSU)
KPN	0.90	−0.0013
KTN	0.89	−0.0008
PWN	1.16	−0.0037
MYN	0.87	−0.0014
GIN	0.76	−0.0007
KPP	0.87	0.0157
KTP	0.87	0.0176
PWP	1.10	0.0184
MYP	0.85	0.0169
GIP	0.75	0.0202

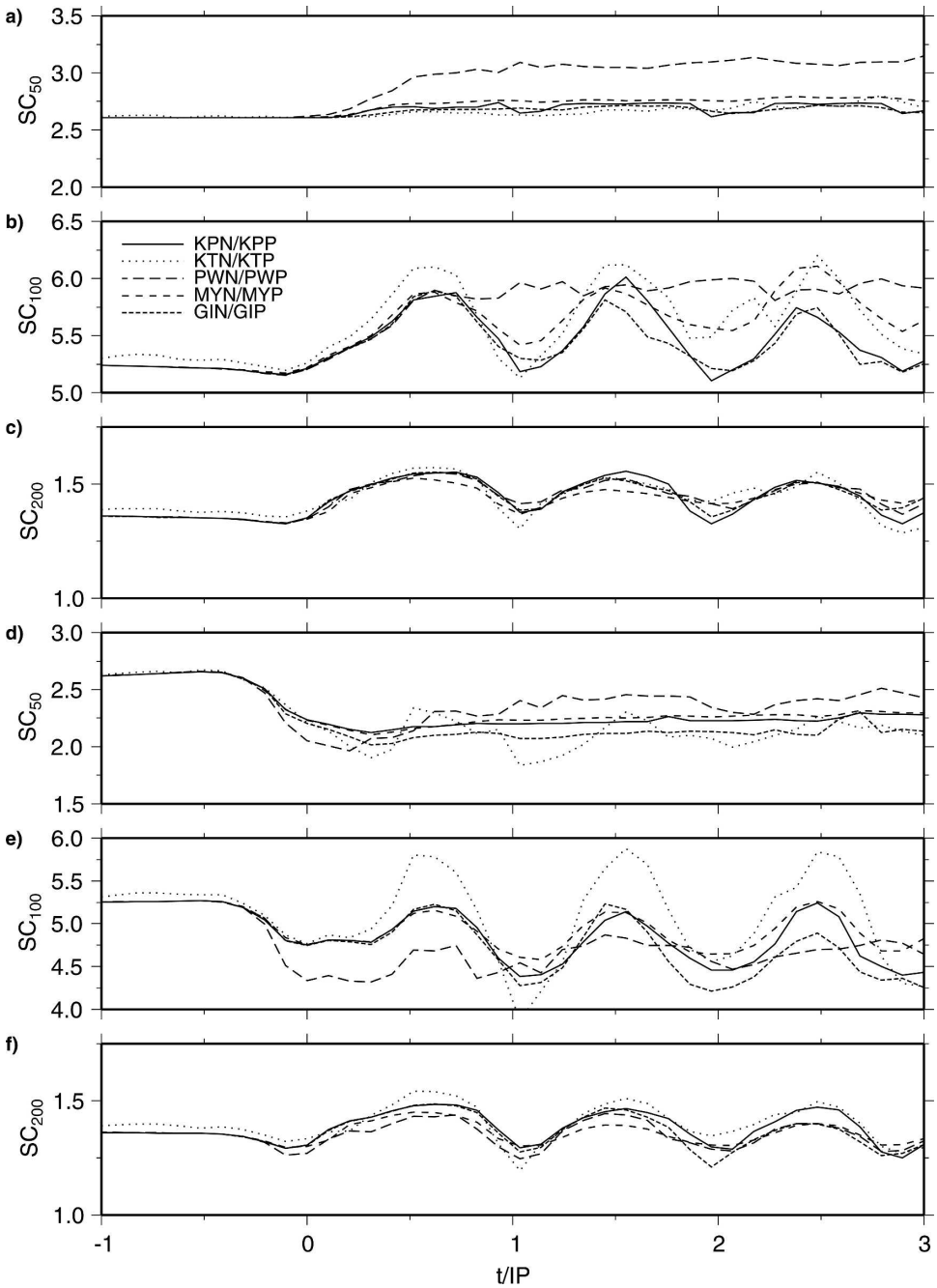

FIG. 11. Evolution of upper-ocean salt content (kg m^{-2}) at a location $2R_{max}$ to the right of the storm track in the Gulf of Mexico for all the 10 cases. The salt content with no precipitation forcing in the top (a) 50 ($\times 10^{-1}$), (b) 100 ($\times 10^{-1}$), and (c) 200 ($\times 10^{-2}$) m, and with precipitation forcing in the top (d) 50 ($\times 10^{-1}$), (e) 100 ($\times 10^{-1}$), and (f) 200 ($\times 10^{-2}$) m.

between cases GIP and PWP suggests that the choice of mixing scheme is more important than freshwater forcing. While more saline mixed layers are seen in cases PWN and PWP at $2R_{max}$ due to stronger simulated mixing, the mixed layer in case KPP is saltier than others in the directly forced region with precipitation forcing.

The heat and salt contents in the upper ocean are also quantified from the simulated fields with respect to three reference depths of 50, 100, and 200 m. Strong mixing in the upper ocean modulates both the heat and salt contents in the upper 50 m. However, because of the minimal mixing from below, near-inertial pumping

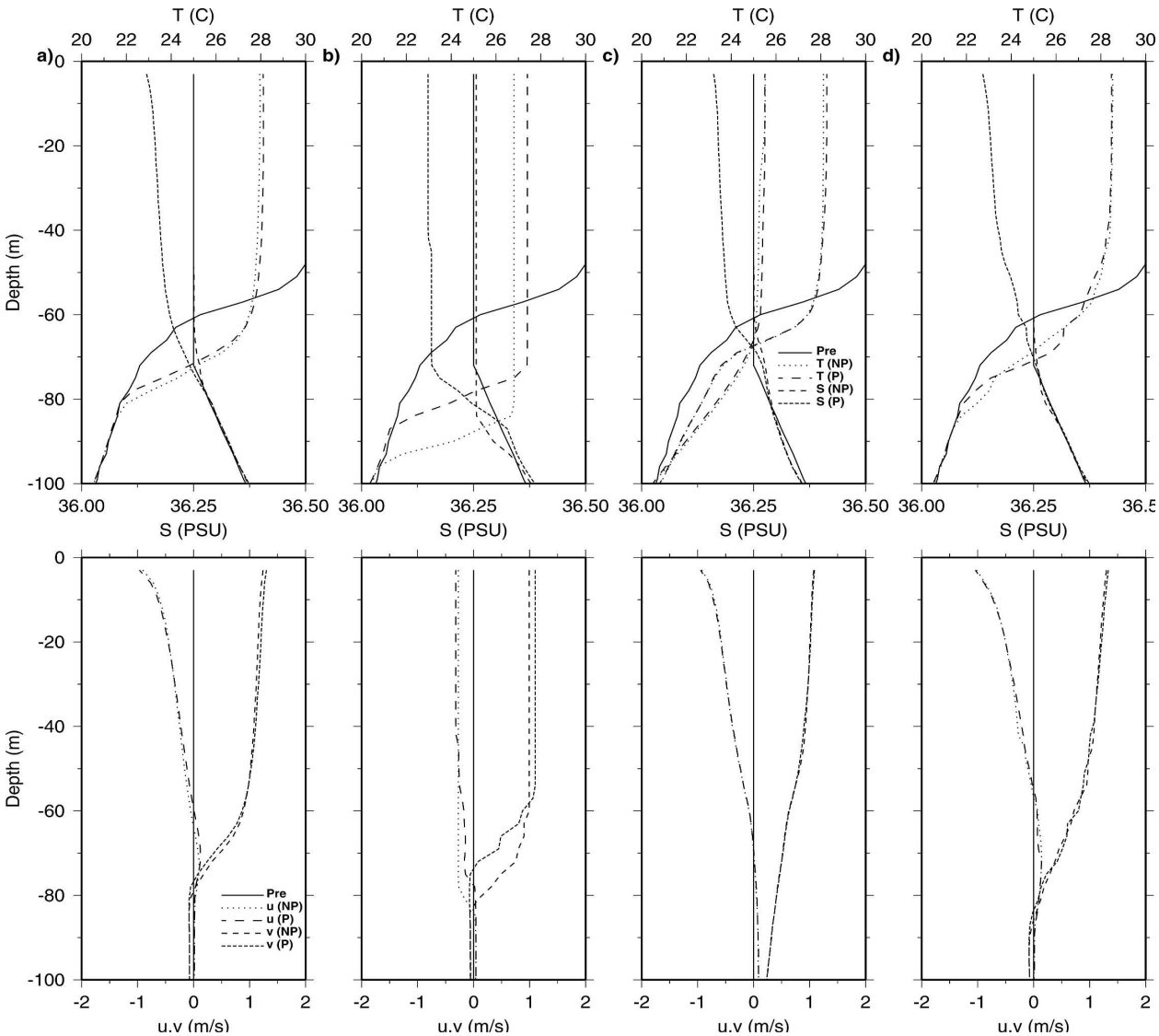

FIG. 12. Vertical structure of the ocean (top) temperature and salinity, and (bottom) current response at a location $2R_{max}$ to the right of the storm track in the directly forced region (at 0 t/IP) in cases (a) KPN, KPP; (b) PWN, PWP; (c) MYN, MYP; and (d) GIN, GIP.

of isotherms and isohalines due to diverging horizontal currents strongly modulate the heat and salt contents estimated with reference depths of 100 and 200 m. The integrated salt storage rates for all 10 experiments are shown in Fig. 11. Clearly, the salt content is affected strongly by mixing in the top 50 m and to a smaller extent in the top 100 m (Figs. 11a,b,d,e) similar to the evolution of MLS, whereas the oscillation at near-inertial period is indicative of the modulation by the inertial pumping due to the diverging and converging horizontal currents in the 200-m estimates.

c. Vertical structure

One of the advantages of higher-order vertical mixing parameterizations with high vertical resolution is that the variability within the mixed layer can be investigated. In particular, vertical mixing of freshwater has been the focus of many observational efforts (Wijesekera et al. 1999). During the TOGA COARE intensive observational periods, observations were acquired to understand the vertical mixing and spreading of the freshwater due to intense rain. Here, structure in the top 100 m is examined during and two days after the storm's passage at a location $2R_{max}$ to the right of the storm track (Figs. 12 and 13). As mentioned earlier, MLT is not significantly affected by precipitation for the three higher-order schemes; however, for the quasi-slab PWP scheme a difference of more than 0.5°C is seen at the point of closest approach of the storm center (Fig. 12b). Clearly, there is a well-defined structure in

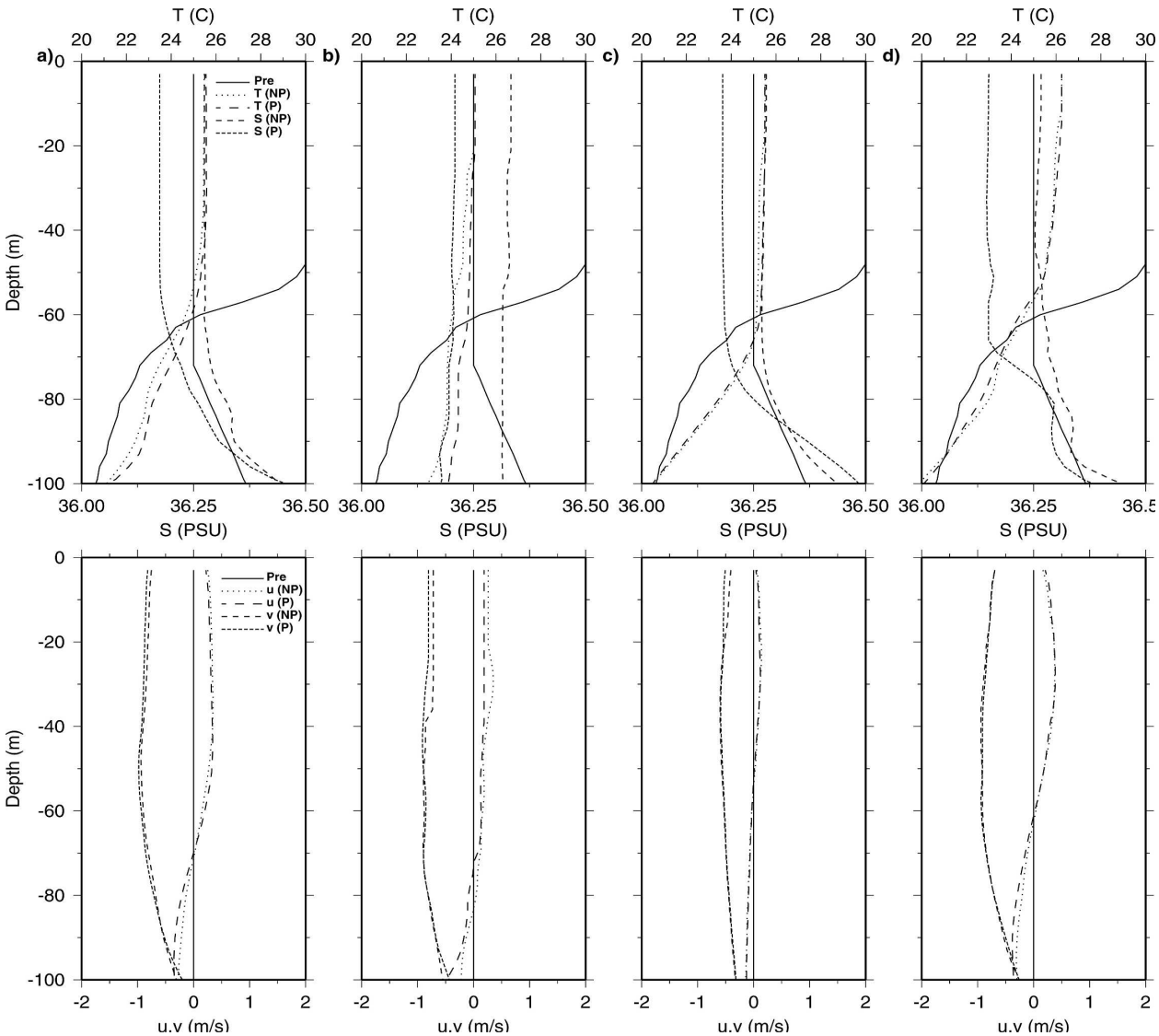

FIG. 13. Same as in Fig. 12, but during the relaxation stage (at 1.6 *t*/IP) in cases (a) KPN, KPP; (b) PWN, PWP; (c) MYN, MYP; and (d) GIN, GIP.

the salinity with the near-surface values being fresher than the ones below with precipitation forcing in cases KPP, MYP, and GIP (Figs. 12a,c,d), though the magnitude is small. Additionally, a clockwise rotation of the currents with depth is also seen in all the higher-order schemes indicating downward energy propagation. Such a trend is maintained even two days after the storm passage though the mixed layer has become homogeneous (Fig. 13). Clearly, in the PWN and PWP cases, strong mixing leads to a nearly homogeneous upper 100 m two days after the storm's passage (Fig. 13b). This is due to the generation of an isothermal layer below the mixed layer due to the gradient Richardson numbers falling below the critical value of 0.25 in the directly forced region. The transition between the mixed layer and this isothermal layer gets eroded by a developing static instability leading to this very deep layer during the relaxation stage. By contrast, simulated mixed layers in the MYN and MYP cases are the shallowest among these four schemes (Figs. 12c and 13c). Similar to the PWP scheme, the KT scheme is also designed to maintain a uniform mixed layer in the model and the mixed layer depths remain the shallowest in cases KTN and KTP (not shown). While simulated vertical profiles in cases KPN, KPP, MYN, and MYP are smooth, these profiles are noisier in the GIN and GIP cases (Figs. 12d and 13d) due to closure approximations in the different dynamic regimes. Addi-

tionally, as seen from Figs. 12c and 13c, simulated currents in MYN and MYP, decayed faster compared to the other mixing schemes. This is perhaps due to a higher dissipation in the MY case.

4. Summary and conclusions

The hybrid coordinate ocean model initialized with quiescent conditions and configured in a Gulf of Mexico domain is used to understand the effects of precipitation on the upper-ocean response during a tropical cyclone passage. As the model has a choice of five different mixing parameterizations, sensitivity of the simulated response to these schemes is also investigated. Wind forcing associated with Hurricane Gilbert in the Gulf of Mexico along with derived precipitation rates based on satellite climatology provides the forcing conditions in these simulations. With the temperature of rainfall being the same as the mixed layer temperature, results indicate a small variability in the simulated MLT for four of the five mixing schemes considered. However, the results for the PWP scheme show a difference of more than 0.5°C. Although the MLT values in the precipitation forced cases are higher due to the freshwater-induced higher stability and the associated reduction in mixing, sensible heat loss due to colder precipitation temperatures does not have a large effect on the MLT. However, simulated MLS is more sensitive to the freshwater forcing. MLS without precipitation tends to be more saline with respect to prestorm values due to mixing from below whereas with added precipitation simulated MLS tends to be fresher. Similar to the MLT evolution, MLS in the PWP scheme is more saline due to enhanced mixing without precipitation that becomes comparable to other schemes when freshwater forcing is added. However, differences between results for the five mixing schemes are much larger than those induced by precipitation. While the momentum response is comparable between the schemes, surface fluxes to the atmosphere vary by more than 300 W m^{-2} between the schemes. This result highlights the need to evaluate the different mixing schemes in comparison with data to identify more appropriate schemes for use in coupled predictive models. Using ocean data acquired in three major hurricanes, these mixing schemes are currently being evaluated that will be the focus of a forthcoming paper.

Acknowledgments. This research was supported by the NASA Goddard Space Flight Center. S. D. Jacob gratefully acknowledges partial support from the NOAA/Joint Hurricane Testbed through Grant NA03OAR4310174 and thanks Dr. David Le Vine of NASA GSFC for his support. Both authors thank Drs. F. Marks (NOAA/HRD, Miami) and M. Lonfat (RMS, London) for their help with the hurricane precipitation climatology. Thanks are due to Drs. A. Wallcraft (Naval Research Lab, Stennis Space Center) and G. Halliwell (RSMAS, University of Miami) for their help with the model. Thanks are also due to Dr. Nick Shay (RSMAS) for many useful discussions on the subject.

REFERENCES

Anderson, S. P., A. Hinton, and R. A. Weller, 1998: Moored observations of precipitation temperature. *J. Atmos. Oceanic Technol.,* **15,** 979–986.

Bender, M. A., I. Ginis, and Y. Kurihara, 1993: Numerical simulations of tropical-cyclone interaction with a high-resolution coupled model. *J. Geophys. Res.,* **98,** 23 245–23 263.

Black, P. G., 1983: Ocean temperature change induced by tropical cyclones. Ph.D. dissertation, The Pennsylvania State University, University Park, PA, 278 pp.

Bleck, R., 2002: An oceanic general circulation model framed in hybrid isopycnic-Cartesian coordinates. *Ocean Modell.,* **4,** 55–88.

Canuto, V. M., A. Howard, Y. Cheng, and M. S. Dubovikov, 2001: Ocean turbulence. Part I: One-point closure model—Momentum and heat vertical diffusivities. *J. Phys. Oceanogr.,* **31,** 1413–1426.

——, ——, ——, and ——, 2002: Ocean turbulence. Part II: Vertical diffusivities of momentum, heat, salt, mass and passive scalars. *J. Phys. Oceanogr.,* **32,** 240–264.

Chang, S. W., and R. A. Anthes, 1978: Numerical simulations of the ocean's nonlinear baroclinic response to translating hurricanes. *J. Phys. Oceanogr.,* **8,** 468–480.

Gaspar, Ph., 1988: Modeling the seasonal cycle of the upper ocean. *J. Phys. Oceanogr.,* **18,** 161–180.

Gosnell, R., C. W. Fairall, and P. J. Webster, 1995: The sensible heat of rainfall in the tropical ocean. *J. Geophys. Res.,* **100,** 18 437–18 442.

Halliwell, G. R., Jr., 2004: Evaluation of vertical coordinate and vertical mixing algorithms in the HYbrid-Coordinate Ocean Model (HYCOM). *Ocean Modell.,* **7,** 285–322.

Jacob, S. D., and L. K. Shay, 2003: The role of oceanic mesoscale features on the tropical cyclone induced mixed layer response. *J. Phys. Oceanogr.,* **33,** 649–676.

——, ——, A. J. Mariano, and P. G. Black, 2000: The 3D oceanic mixed layer response to hurricane Gilbert. *J. Phys. Oceanogr.,* **30,** 1407–1429.

Kraus, E. B., and J. S. Turner, 1967: A one-dimensional model of the seasonal thermocline. II: The general theory and its consequences. *Tellus,* **19,** 98–105.

Large, W. G., and S. Pond, 1981: Open ocean momentum flux measurements in moderate to strong wind. *J. Phys. Oceanogr.,* **11,** 324–336.

——, J. C. McWilliams, and S. C. Doney, 1994: Oceanic vertical mixing: A review and a model with a nonlocal boundary layer parameterization. *Rev. Geophys.,* **32,** 363–403.

Lonfat, M., F. D. Marks Jr., and S. S. Chen, 2004: Precipitation distribution in tropical cyclones using the Tropical Rainfall Measuring Mission (TRMM) Microwave Imager: A global perspective. *Mon. Wea. Rev.,* **132,** 1645–1660.

Marks, F. D., and L. K. Shay, 1998: Landfalling tropical cyclones:

Forecast problems and associated research opportunities. *Bull. Amer. Meteor. Soc.,* **79,** 305–323.

——, G. Kappler, and M. DeMaria, 2002: Development of a tropical cyclone rainfall climatology and persistence (R-CLIPER) model. Preprints, *25th Conf. on Hurricanes and Tropical Meteorology,* San Diego, CA, Amer. Meteor. Soc., 327–328.

Mellor, G. L., and T. Yamada, 1982: Development of a turbulence closure model for geophysical fluid problems. *Rev. Geophys. Space Phys.,* **20,** 851–875.

Miller, B. I., 1958: Rainfall rates in Florida hurricanes. *Mon. Wea. Rev.,* **86,** 258–264.

Powell, M. D., and S. H. Houston, 1996: Hurricane Andrew's landfall in south Florida. Part II: Surface wind fields and potential real-time applications. *Wea. Forecasting,* **11,** 329–349.

——, P. J. Vickery, and T. A. Reinhold, 2003: Reduced drag coefficient for high wind speeds in tropical cyclones. *Nature,* **422,** 279–283.

Price, J. F., 1981: Upper ocean response to a hurricane. *J. Phys. Oceanogr.,* **11,** 153–175.

——, R. A. Weller, and R. Pinkel, 1986: Diurnal cycling: Observations and models of the upper ocean response to diurnal heating, cooling, and wind mixing. *J. Geophys. Res.,* **91,** 8411–8427.

Pudov, V. I., and I. Ginis, 2000: Sea surface salinity reduction in the upper ocean induced by tropical cyclones. Preprints, *10th Conf. on Interaction of the Sea and Atmosphere,* Ft. Lauderdale, FL, Amer. Meteor. Soc., J72–J73.

Shay, L. K., and S. D. Jacob, 2006: Relationship between oceanic energy fluxes and surface winds during tropical cyclone passage. *Atmosphere–Ocean Interactions,* W. Perrie, Ed., Vol. II, WIT Press, 115–137.

——, P. G. Black, A. J. Mariano, J. D. Hawkins, and R. L. Elsberry, 1992: Upper ocean response to hurricane Gilbert. *J. Geophys. Res.,* **97** (C12), 20 277–20 248.

Wijesekera, H. W., C. A. Paulson, and A. Huyer, 1999: The effect of rainfall on the surface layer during a westerly wind burst in the western equatorial Pacific. *J. Phys. Oceanogr.,* **29,** 612–632.